Journal of Applied Mathematics and Physics, 2023, 11, 3484-3504
https://www.scirp.org/journal/jamp
ISSN Online: 2327-4379
ISSN Print: 2327-4352

Computational Dynamics of Stagnation Point Flow of Micropolar Fluid Past Vertical Porous Plates

Ayando Timothy*, Ibrahim Y. Seini, Musah Sulemana

Faculty of Physical Sciences, University for Development Studies, Tamale, Ghana
Email: *tayando@uds.edu.gh

How to cite this paper: Timothy, A., Seini, I.Y. and Sulemana, M. (2023) Computational Dynamics of Stagnation Point Flow of Micropolar Fluid Past Vertical Porous Plates. *Journal of Applied Mathematics and Physics*, **11**, 3484-3504.
https://doi.org/10.4236/jamp.2023.1111221

Received: June 25, 2023
Accepted: November 18, 2023
Published: November 21, 2023

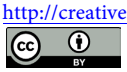

Abstract

This work examines the flow of a micropolar fluid over a vertical porous plate at the MHD stagnation point under viscous dissipation, convective boundary conditions, and thermal radiation. The governing partial differential equations and a set of similarity parameters were used to transform them into ordinary differential equations. The Runge-Kutta fourth-order algorithm is used in conjunction with the Newton Raphson shooting technique to numerically solve the generated self-similar equations. Results were tabulated both numerically and graphically, and examples for different controlling factors are quantitatively analyzed. According to the study, the vortex viscosity parameter (k) causes the velocity profiles to rise while the magnetic parameter, suction parameter, and radiation parameter cause them to fall. In contrast, as the flow's suction and prandtl values rise, so do the magnetic parameter, radiation, and vortex viscosity, while the thickness of the thermal boundary layer decreases.

Keywords

MHD, Viscous Dissipation, Thermal Radiation, Microrotation, Micropolar Fluid

1. Introduction

Fluids having microstructure are known as micropolar fluids. They fall under the category of fluids known as polar fluids, which have nonsymmetric stress tensors. Erigen [1] first proposed the fundamental continuum theory for this group of fluids and has been a well-liked subject of study. The movement of fluids with suspensions, colloidal fluids, polymer, bodily fluids, blood, and liquid

crystals are all explained by this hypothesis. Incompressible micropolar boundary layer flow over a semi-infinite plate was researched by Ahmadi [2]. In their investigation of the heat transfer on continuously rotating plates in micropolar fluids, Soundalgekar and Takhar [3] discovered the impact of surface temperature on the fluid dynamics. Similar to this, Hayat and Ali [4] explored the peristaltic flow of micropolar fluid in an asymmetric channel as well as the nature of the endoscope. Rees and Pop [5] studied the flow of a micropolar fluid on a continuously moving plate, whereas Sajid *et al.* [6] looked at the homotopy analysis for boundary layer flow of micropolar fluid via porous channels. The mixed convection flow of micropolar fluid across a non-linearly expanding surface was further investigated by Hayat *et al.* [7].

In many technical applications, such as the design of radial diffusers, thrust bearing, thermal oil recovery and transpiration cooling, stagnation point flow is crucial. Hiemenz [8] employed a similarity transformation method to convert the Navier-Stokes equations to nonlinear ordinary differential equations and made the discovery of stagnation point flow. Homann [9] expanded on this issue by incorporating the axisymmetric stagnation point scenario in both two and three dimensional instances. In addition to making a substantial contribution to the stagnation-point flow of micropolar fluid towards a stretched surface, Nazar *et al.* [10] also added to our understanding of the flow dynamics of stagnation point flow.

The design of several inventive energy conversion devices that run at high temperature has a significant problem from thermal radiation. The emissions from heated walls and working fluid are principally caused by the effects of thermal radiation. Several research investigations, like those by Zhu *et al.* [11] and Pop *et al.* [12], have discussed the effects of radiation. While Seini and Makinde [13] looked at the impact of radiation on chemically reacting MHD boundary layer flow via a vertical porous plate, Christian *et al.* [14] examined MHD stagnation flow with chemical reaction and radiation toward a heated shrinking porous surface. T. Ayando [15] also looked into the Blasius flow of MHD micropolar fluid caused by heat radiation through a permeable plate.

Viscous dissipation's function is to alter the temperature distribution by acting as energy source, which impacts heat transfer rates. Whether the sheet is being heated or cooled determines the benefits of the viscous dissipation effect. The impact of viscous dissipation in a heated vertical plate with natural convection was examined by Pantokratoras [16]. The effects of suction and viscous dissipation on MHD boundary layer flow in a porous material over a moving vertical plate were also explored by Lakshmi *et al.* [17]. The effects of viscous and ohmic dissipation on heat transfer and viscoelastic MHD flow across a stretched sheet were next investigated by Subhas *et al.* [18]. Imoro *et al.* [19] investigated the presence of viscous dissipation and nth order chemical reaction on heat and mass transfer over a vertical surface with convective boundary conditions, whereas Arthur *et al.* [20] examined the presence of radiation with viscous dissipa-

tion and convective boundary condition chemically reacting hydromagnetic flow over a flat surface. Makinde [21] investigated internal heat generation and convective boundary conditions on a moving vertical plate with natural convection using the similarity solution method.

The stagnation point flow of an MHD micropolar fluid in the presence of melting processes and heat absorption was studied by Mamta *et al.* [22], who found that the heat transfer rate reduces with melting and heat absorption. He said that at the fluid-solid boundary, heat production parameters greatly rise, while Lok *et al.* [23] looked the mixed convection flow of micropolar fluid at the stagnation point on a vertical surface and Ramachandra *et al.* [24] studied the mixed convection stagnation point flows close to a vertical porous surface.

Ghasemi *et al.* [25] investigated the effects of solar radiation on MHD stagnation point flow and heat transfer across a stretched sheet.

Lund *et al.* [26] investigated the dual similarity solution of MHD stagnation point flow of casson fluid with thermal radiation and viscous dissipation effects. Hsio [27] studied the stagnation electrical MHD nanofluid mixed convection with slip boundary on stretching sheet, while Bilal [28] examined the micropolar flow of electrical MHD nanofluid with nonlinear thermal radiation and slip effects. Both researchers discovered that increasing the magnetic parameter (M) or electrical parameter (E) results in an increase in temperature distribution at a specific point of the flow region. Furthermore, Shahzada *et al.* [29] also expanded on Hsiao [27] research by looking at the stagnation point flow of an EMHD micropolar nanofluid with mixed convection and slip boundary. Recent studies by Ishak *et al.* [30] and Olanrewaju *et al.* [31] examined the effects of thermal radiation on magnetohydrodynamic (MHD) flow of micropolar fluid towards a stagnation point on a vertical surface and found that thermal radiation and absorption has greater impact on the velocity, angular velocity and temperature field.

To the best of the authors' knowledge, there is no documentation of the interaction of viscous dissipation, thermal radiation, and convective boundary conditions of stagnation point flow of micropolar fluid via vertical porous plate in the literature that is currently accessible.

This study investigates the impact of convective boundary condition, viscous dissipation, and thermal radiation on stagnation point flow of micro polar fluid through a vertical porous plate. The practical applications of this research include the extraction of polymers in melt-spinning processes, the cooling of nuclear reactors during emergency shutdown, and the cooling of electronic devices, serve as the driving force behind it.

2. Mathematical Model

On a heated vertical surface, a constant laminar two-dimensional flow of a viscous incompressible electrically conducting micropolar fluid through a porous media has been taken into consideration. Our research took into account the

tangential and normal velocity components, as well as the x-axis running parallel to the wall in the direction of the flow motion and y-axis perpendicular to it. We also failed to consider the generated magnetic field that the movement of the electrically conducting fluid caused. The following steps are taken to get the boundary layer equations representing the flow:

$$\frac{\partial u}{\partial x}+\frac{\partial v}{\partial y}=0 \tag{1}$$

$$u\frac{\partial u}{\partial x}+v\frac{\partial u}{\partial y}=U\frac{\mathrm{d}U}{\mathrm{d}x}+\left(\frac{\mu+k}{\rho}\right)\frac{\partial^2 u}{\partial y^2}+\frac{k}{\rho}\frac{\partial H}{\partial y}+\frac{\sigma B_0^2(x)}{\rho}\left(u-U\right)+g\beta\left(T-T_\infty\right) \tag{2}$$

$$\rho j\left(u\frac{\partial H}{\partial x}+v\frac{\partial H}{\partial y}\right)=\gamma\frac{\partial^2 H}{\partial y^2}-k\left(2H+\frac{\partial u}{\partial y}\right) \tag{3}$$

$$\rho C_p\left(u\frac{\partial T}{\partial x}+v\frac{\partial T}{\partial y}\right)=\kappa\frac{\partial^2 T}{\partial y^2}+\mu\left(\frac{\partial u}{\partial y}\right)^2-\frac{\partial q_r}{\partial y} \tag{4}$$

With boundary conditions:

$$\text{At}\quad y=0:\ u=0, v=-V, H=-\frac{1}{2}\frac{\partial u}{\partial y}, \kappa\frac{\partial T}{\partial y}=-h_w\left(T_w-T\right)$$

$$\text{As}\quad y\to\infty:\ u\to U, H\to 0, T\to T_\infty \tag{5}$$

where u and v are the x and y-axis velocity components, respectively, g is the acceleration caused by gravity, T is the fluid temperature in the boundary layer, k is the vortex viscosity, μ is the dynamic viscosity, κ is the thermal conductivity, ρ is the fluid density, β is the thermal expansion coefficient, j is the microinertia density, H is the microrotation vector.

We further assume that $K=\frac{k}{\mu}$ is the vortex viscosity parameter where the field of equations predicts proper behavior of the vortex when the microstructure effects are insignificant.

Using Rosseland approximation for radiative, simplified the radiated heat flux to:

$$q_r=-\frac{4\sigma^*}{3K'}\frac{\partial T^4}{\partial y}, \tag{6}$$

where K' and σ^* are mean absorption coefficient and Stefan-Boltzmann constant. The term T^4 may be expressed as a linear function of temperature difference within the flow. Hence, in a Taylor series expansion about T_∞ and neglecting higher order terms, we get;

$$T^4\cong 4T_\infty^3T-3T_\infty^4. \tag{7}$$

Introducing the following dimensionless quantities:

$$\psi\left(x,y\right)=x\sqrt{a\upsilon}f\left(\eta\right),\quad \eta=y\sqrt{\frac{a}{\upsilon}},\quad \theta\left(\eta\right)=\frac{T-T_\infty}{T_w-T_\infty},\quad H\left(x,y\right)=U\sqrt{\frac{a}{\upsilon}}h\left(\eta\right) \tag{8}$$

where ψ, θ, h *and* υ are respectively stream function, temperature, dimensionless microrotation and kinematic viscosity.

Noting the usual relationship of the velocity components $u = \frac{\partial \psi}{\partial y}$, $v = -\frac{\partial \psi}{\partial x}$, satisfies the continuity Equation (1) identically.

Equations (2)-(4) and the boundary conditions in (5) are transformed into non-linear higher order differential equations in the form:

$$(1+K)f''' + ff'' + M(1-f') - f'^2 + \lambda\theta + Kh' = -1, \tag{9}$$

$$\left(1+\frac{K}{2}\right)h'' + fh' - hf' - K(2h+f'') = 0. \tag{10}$$

$$\left(1+\frac{4}{3}Ra\right)\theta'' + Pr(f\theta' - f'\theta) + Brf''^2 = 0, \tag{11}$$

The transformed boundary conditions are;

$$\begin{aligned} &f'(0) = 0,\ f(0) = fw,\ h(0) = -\frac{1}{2}f''(0),\ \theta'(0) = Bi(\theta(0)-1), \\ &f'(\infty) = 1,\ h(\infty) = 0,\ \theta(\infty) = 0 \end{aligned} \tag{12}$$

where $j = \upsilon/a$ is the characteristic length, $Gr_x = g\beta_T(T_w - T_\infty)x^3/\upsilon^2$ is the local thermal Grashof number, $Br = \mu U^2/\kappa(T_w - T_\infty)$ term as Brinkmann number, $Pr = \upsilon/\alpha$ Prandtl number, $M = \sigma B_0^2/\rho a$ represents as magnetic field term, $fw = \frac{v}{\sqrt{a\upsilon}}$ as suction term, $Ra = 4\sigma^* T_\infty^3/\kappa K'$ represents the thermal radiation parameter, $\lambda = Gr_x/Re_x^2$ term as the buoyancy, $Re_x = Ux/\upsilon$ local Reynolds number, $Bi = \frac{h_w}{\kappa}\sqrt{\frac{\upsilon}{a}}$ represents convective heat transfer parameter.

3. Numerical Procedure

The higher order ordinary differential Equations (9) through (11) and the associated transformed boundary conditions (12) are reduced to a coupled first order system of ODEs using the standard Newton-Raphson shooting method and the fourth-order Runge-Kutta integration algorithm to arrive at the numerical solution. We employ numerical shooting technique where the two ending boundary conditions are utilized to produce two unknown initial conditions at at $\eta = 0$. In this calculation, the step size $\Delta\eta = 0.001$ was used while obtaining the numerical solution with $\eta_{\max} = 10$ and six-decimal (10^{-6}) accuracy as the criterion for convergence.

The following reduction steps are allowed in order:

$$\begin{aligned} &f = x_1,\ f' = x_2,\ f'' = x_3,\ f''' = x_4,\ h = x_5,\ h' = x_6,\ h'' = x_7, \\ &\theta = x_8,\ \theta' = x_9,\ \theta'' = x_{10} \end{aligned}$$

Therefore, equations (9) - (11) can be reduced as first order system as follows:

$$\begin{aligned} f &= x_1, \\ f' &= x_2, \\ f'' &= x_3, \end{aligned}$$

$$f''' = x_4 = \frac{-1 - kx_6 - \lambda x_8 + (x_2)^2 - m(1 - x_1) - x_1 x_3}{1 + K}$$

$$h = x_5,$$

$$h' = x_6,$$

$$h'' = x_7 = \frac{x_5 x_2 - x_1 x_6 + K(2x_3 + x_2)}{1 + \frac{K}{2}}$$

$$\theta = x_8$$

$$\theta' = x_9$$

$$\theta'' = x_{10} = -Pr(x_1 x_9 - x_2 x_8) - Br(x_3)^2$$

The local Nusselt number, couple stress, and plate surface shear stress, which are each represented by the numerical values $f''(0)$, $h'(0)$ and $-\theta'(0)$ are computed numerically and results are shown in tabular form.

For different prandtl number (*pr*) values, the studies of Ramachandran *et al.*, Lok *et al.*, Ishak *et al.*, Olanrewaju *et al.* and the present study are presented in Table 1 and Table 2. The current study is in line with earlier published efforts in the field. The Nusselt number, couple stress, and shear stress values are shown numerically in Table 3. According to the results, the shear stress and the couple stress rise with increasing values of *fw*, *Bi*, *M*, *Ra*, *Br* and λ ($\lambda > 0$), whereas they decrease with rising values of *K*, *Pr* and λ ($\lambda < 0$). At the plate surface, the shear stress and couple stresses are reduced by momentum and angular momentum diffusion, while they are increased by the magnetic field intensity, suction, viscous dissipation, convective heat transfer and thermal radiation.

The correlation between rate of heat transfer and shear stress is seen in Table 4. The impact of buoyant forces results in an increase in shear stress and a decrease in the rate of heat transfer at the surface, as shown numerically in the table.

Table 1. An example of $f''(0)$ results for various values of *Pr* with $\lambda = 1$, $Br = K = Ra = M = 0$, and $Bi_x = 10^7$.

Pr	Ramachandran *et al.* (1988)	Lok *et al.* (2005)	Ishak *et al.* (2008)	Olanrewaju *et al.* (2011)	Present study
0.7	1.7063	1.706376	1.7063	1.7063227120375	1.706322
1	-	-	1.6755	1.6754365718388	1.675436
7	1.5179	1.517952	1.5179	1.5179126193762	1.517912
10	-	-	1.4928	1.4928386730384	1.492838

Table 2. An example of $-\theta(0)$ results for various values of *Pr* with $\lambda = 1$, $Br = K = M = Ra = 0$, and $Bi_x = 10^7$.

Pr	Ramachandran *et al.* (1988)	Lok *et al.* (2005)	Ishak *et al.* (2008)	Olanrewaju *et al.* (2011)	Present study
0.7	0.7641	0.764087	0.7641	0.7640634014961508	0.7640628
1	-	-	0.8708	0.8707786011745782	0.8707778
7	1.7224	1.722775	1.7225	1.7223816064916741	1.7223785
10	-	-	1.9448	1.9446173966286199	1.9446135

Table 3. Nusselt number, shear and couple stress numerical values.

Pr	*M*	*K*	*Λ*	*Ra*	*Br*	*Bi*	*Fw*	$F'(0)$	$H'(0)$	$-\theta'(0)$
0.7	0.1	1.0	1.0	0.1	0.1	0.1	0.1	0.843868	−0.686483	0.082439
1.0								0.830204	−0.693896	0.084694
7.0								0.787947	−0.715068	0.093365
10.0								0.784208	−0.716758	0.094455
	0.5							0.953501	−0.636323	0.084577
	1.0							1.089963	−0.572344	0.084395
		2.0						0.105585	−1.692473	0.083509
		3.0						−0.717965	−2.560938	0.066982
			−2.0					−0.761830	−1.551959	0.012953
			−1.0					−0.791814	−1.599856	−0.062955
			2.0					0.886261	−0.666636	0.084642
			3.0					0.941836	−0.639429	0.084577
				0.5				0.838206	−0.689319	0.083668
				1.0				0.846859	−0.684285	0.082544
					0.5			0.899741	−0.659197	0.069059
					1.0			0.995722	−0.611110	0.046300
						0.5		0.919372	−0.650938	0.290082
						1.0		0.972230	−0.625230	0.418305
							0.5	0.967507	−0.683157	0.087347
							1.0	1.169603	−0.606788	0.089586

Table 4. Shear stress and Nusselt number numerical findings.

Pr	*M*	*Ra*	*Br*	*Bi*	*Fw*	*K*	*λ*	$F'(0)$	$-\theta'(0)$
1.0	0.1	0.1	0.1	0.1	0.1	0	−3	−1.758828	0.011217
1.0	0.1	0.1	0.1	0.1	0.1	0	−2	−1.750451	−0.026879
1.0	0.1	0.1	0.1	0.1	0.1	0	0	1.923517	0.088116
1.0	0.1	0.1	0.1	0.1	0.1	0	1	1.977830	0.087991
1.0	0.1	0.1	0.1	0.1	0.1	0	2	2.032881	0.087861
1.0	0.1	0.1	0.1	0.1	0.1	1	−3	−1.651530	0.010201
1.0	0.1	0.1	0.1	0.1	0.1	1	−2	−1.677709	−0.029515
1.0	0.1	0.1	0.1	0.1	0.1	1	0	1.135961	0.089640
1.0	0.1	0.1	0.1	0.1	0.1	1	1	1.169603	0.089586
1.0	0.1	0.1	0.1	0.1	0.1	1	2	1.203345	0.089539

4. Discussion of Results

4.1. Velocity Profiles

Figures 1-7 shows the velocity curve with various regulating parameters. The

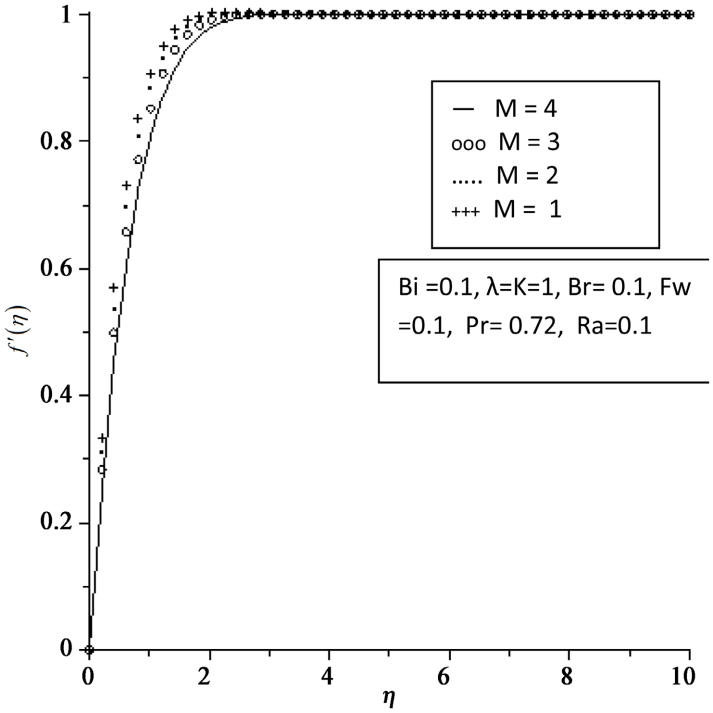

Figure 1. Magnetic field parameter velocity profiles.

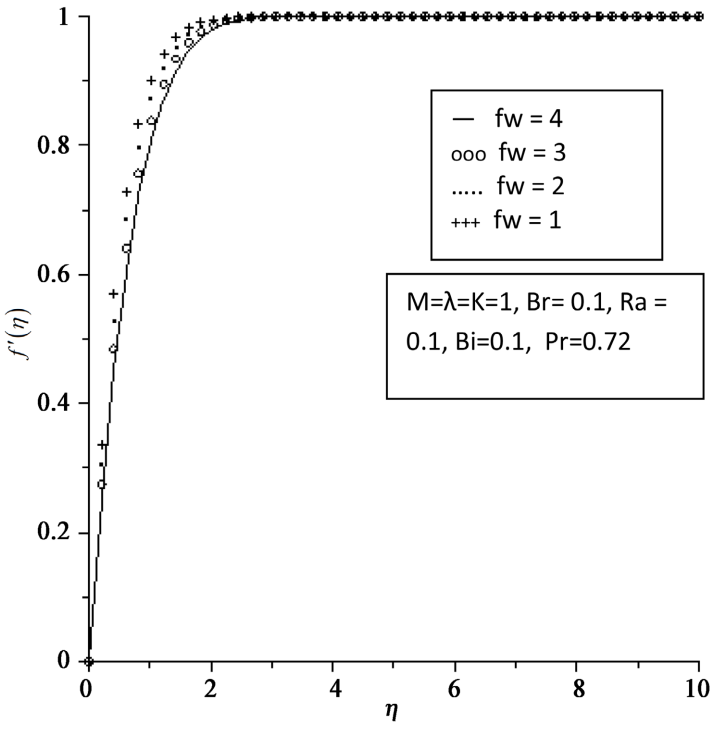

Figure 2. Suction parameter velocity profiles.

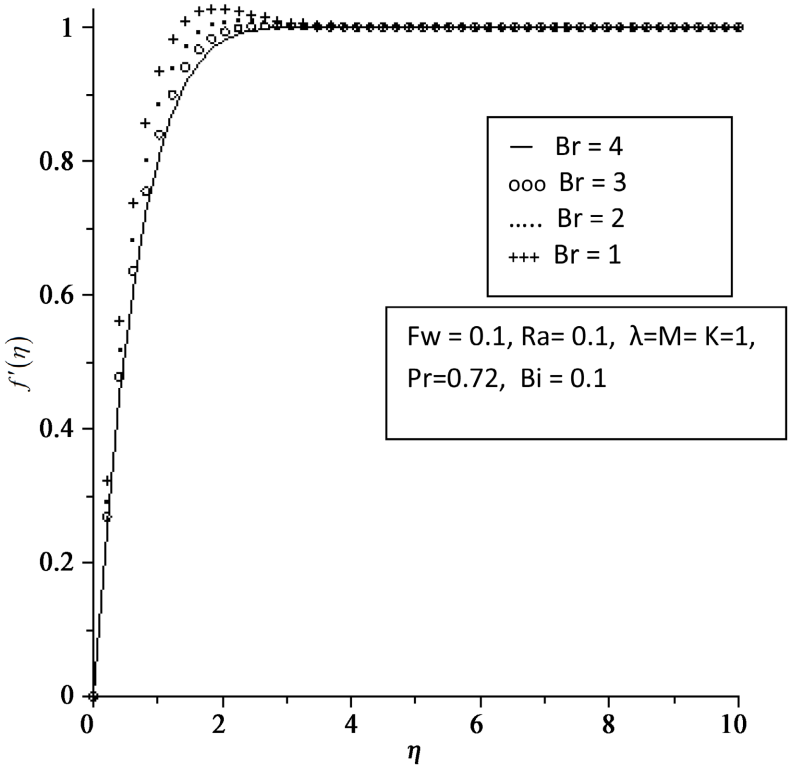

Figure 3. Brinkmann Number velocity profiles.

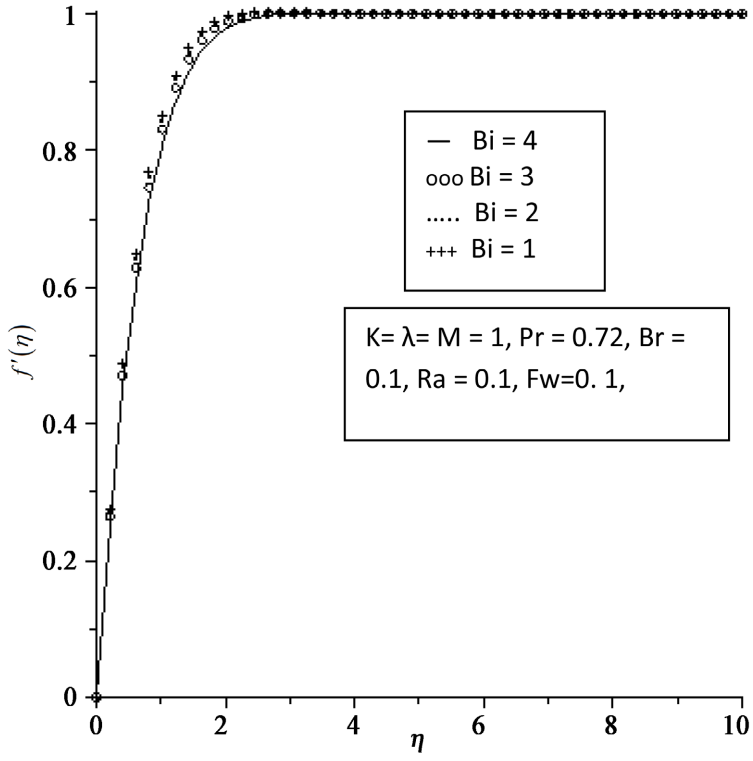

Figure 4. Biot number velocity profiles.

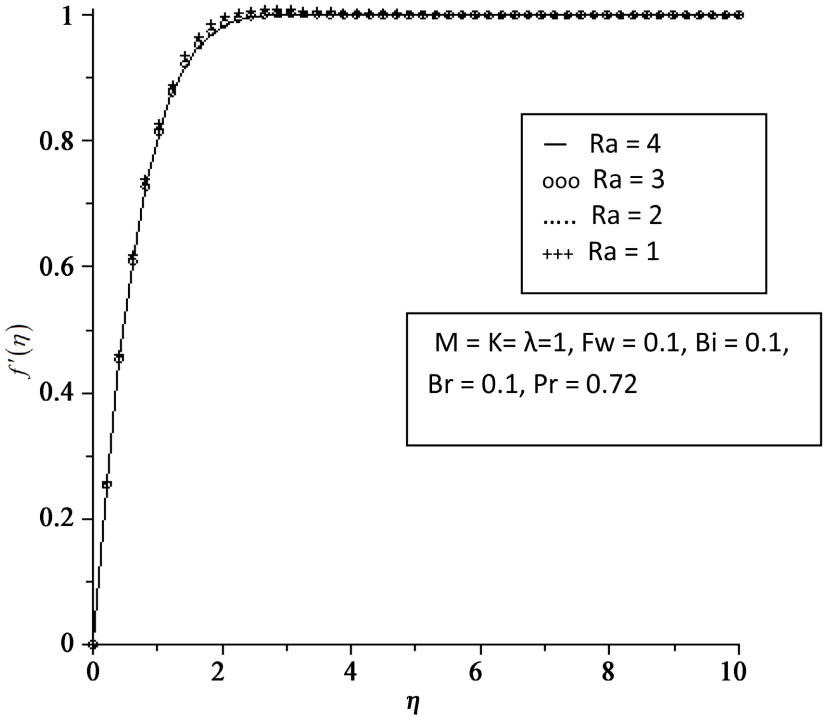

Figure 5. Radiation parameter velocity profiles.

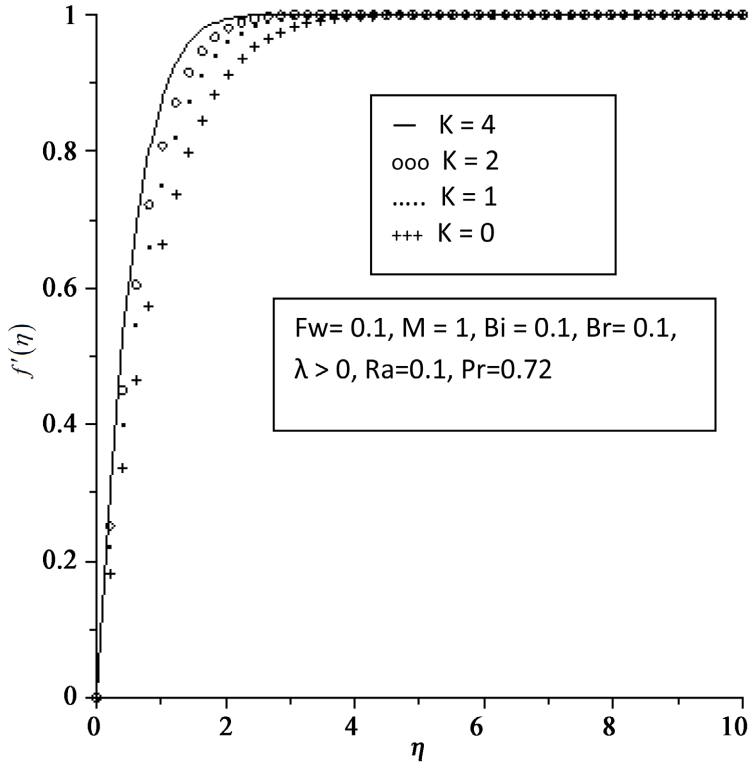

Figure 6. Material parameter velocity profiles (assisting flow).

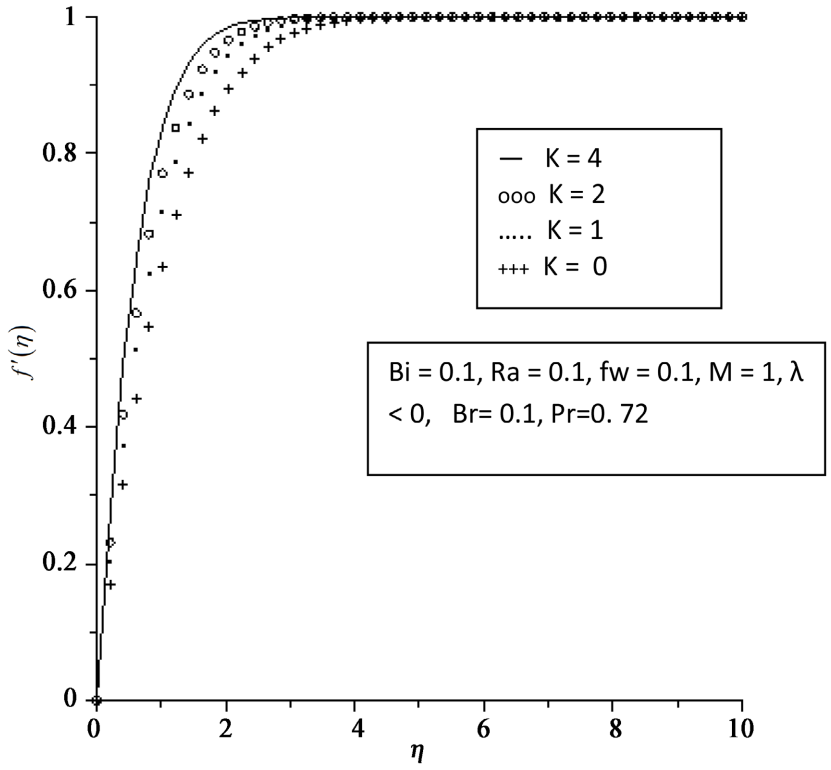

Figure 7. Vortex viscosity parameter velocity profiles (opposing flow).

fluid velocity is typically lowest near the plate surface and rises to the free stream value, which meets the boundary criteria for the distant field. When the magnetic field intensity is increased, the longitudinal velocity consistently decreases, and all profiles asymptotically approach the free stream value away from the plate. This effect is caused by the Lorenz force, which rises as the magnetic field intensity increases and creates more resistance to fluid flow.

Figure 2 shows how the velocity field and suction (*fw*) values vary over boundary layer. Velocity decreases with increasing suction. Suction is a medium that creates flow resistance, slowing the flow velocity. As shown in Figures 3-5, the velocity boundary layer thickness decreases as the values of thermal radiation, Brinkmann number (*Br*) and Biot number (*Bi*) on the velocity increase, respectively, due to viscous dissipation and convective heat transfer. Additionally, as shown in Figure 6 & Figure 7, the thermal boundary layer thickness rises for varying values of the vortex viscosity parameter (*k*), improving the flow kinematics of fluid flows due to an increase in angular momentum diffusion.

4.2. Microrotation Profiles

As seen in Figure 8 & Figure 9, the microrotation profiles decrease as the values of magnetic field (*m*) and suction (*fw*) parameter rise. The Lorenz force, which tends to work against the direction of the fluid flow when there is a magnetic field present, is a drag-like force. As the fluid temperature, magnetic field, and suction rise as result, the fluid velocity and microrotation decrease. Figure 10 &

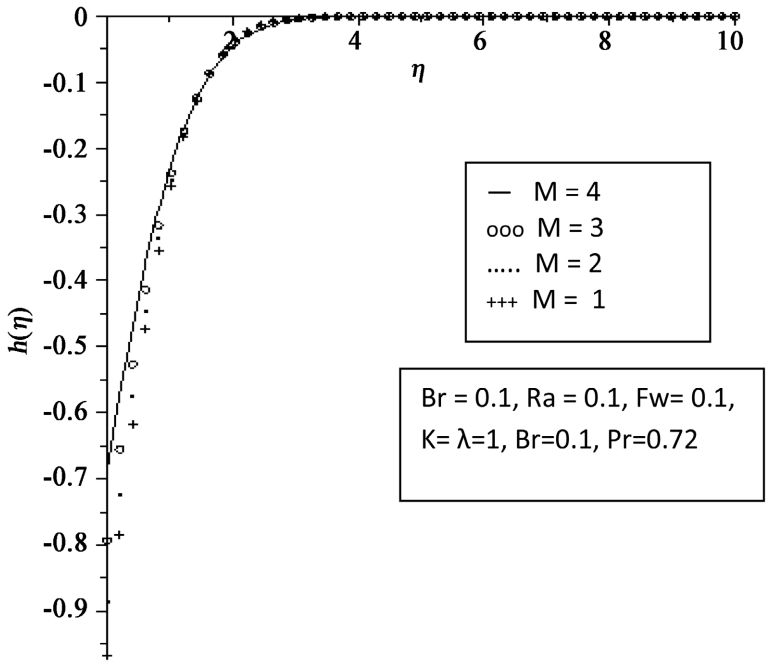

Figure 8. Microrotation profiles for magnetic field parameter.

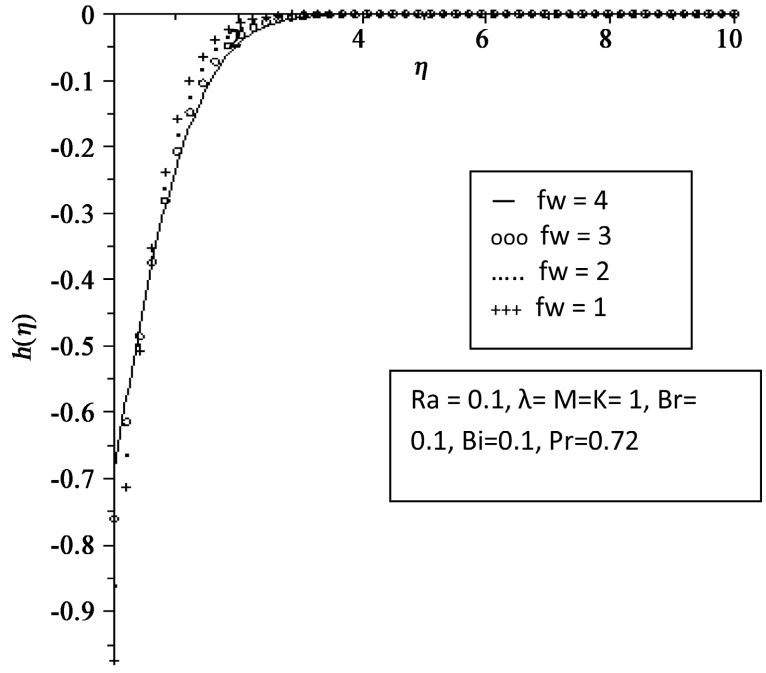

Figure 9. Suction parameter microrotation profiles.

Figure 11 show the microrotation profiles for the Brinkmann (*Br*) and Biot (*Bi*) numbers.

Due to internal heat production from convective heat transfer and viscous dissipation, the microrotation profiles at plate surface decrease as *Br* and *Bi* number rise. Figure 12 & Figure 13 depict the microrotation profiles for the vortex viscosity parameter (*k*) for aiding and opposing flows. As the angular

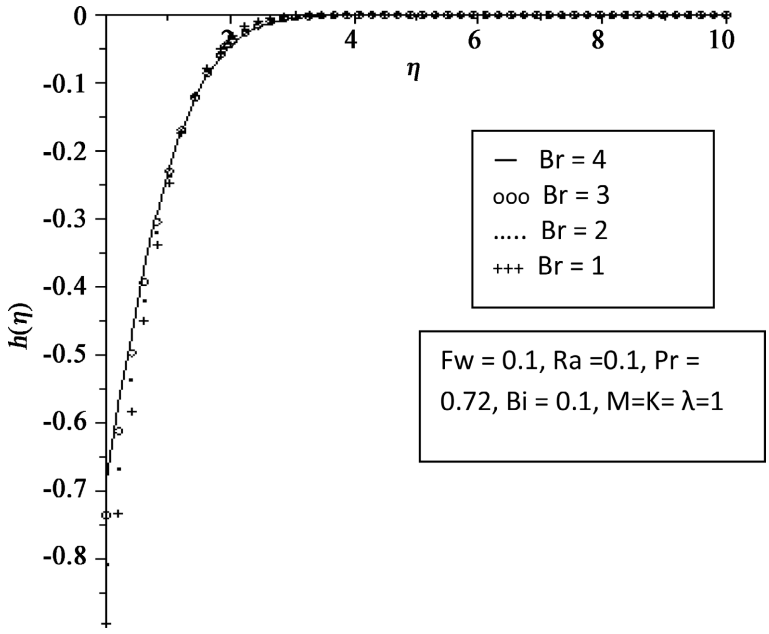

Figure 10. Microrotation profiles for Brinkmann Number.

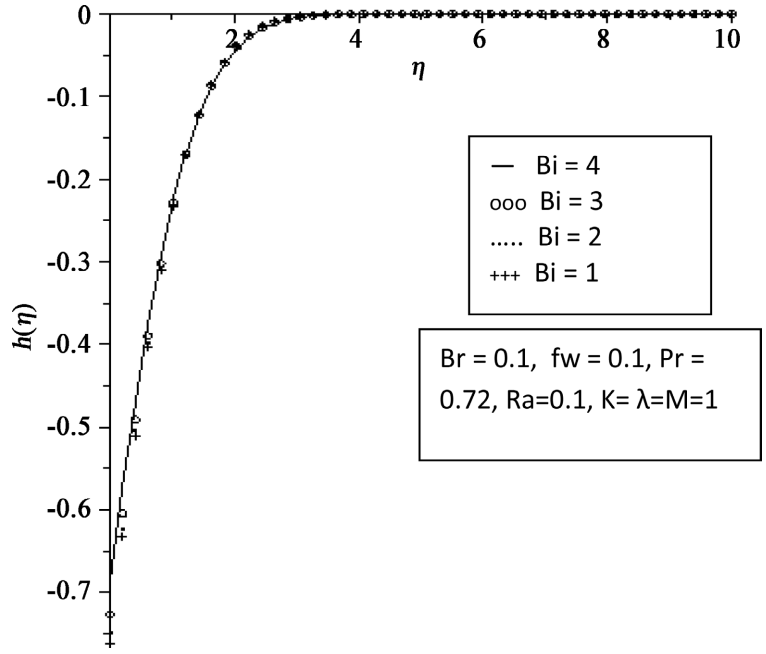

Figure 11. Biot parameter microrotation profiles.

velocity or microrotation rises close to the plate surface, the microrotation profiles rise with increasing values of *R*.

4.3. Temperature Profiles

Figures 14-21 show the changes in temperature profiles. The fluids temperature reaches its peak at the plate surface before decreasing to meet the boundary requirements at free stream temperature. With an increase in the values of magnetic parameter, a drop in temperature profiles is seen. According to Figure 14

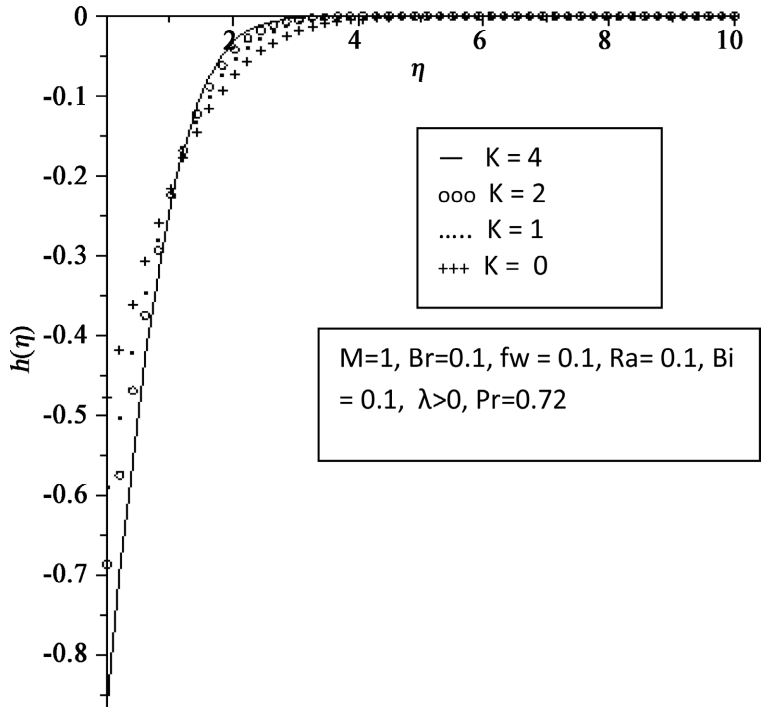

Figure 12. Microrotation profile for vortex viscosity parameter (assisting flow).

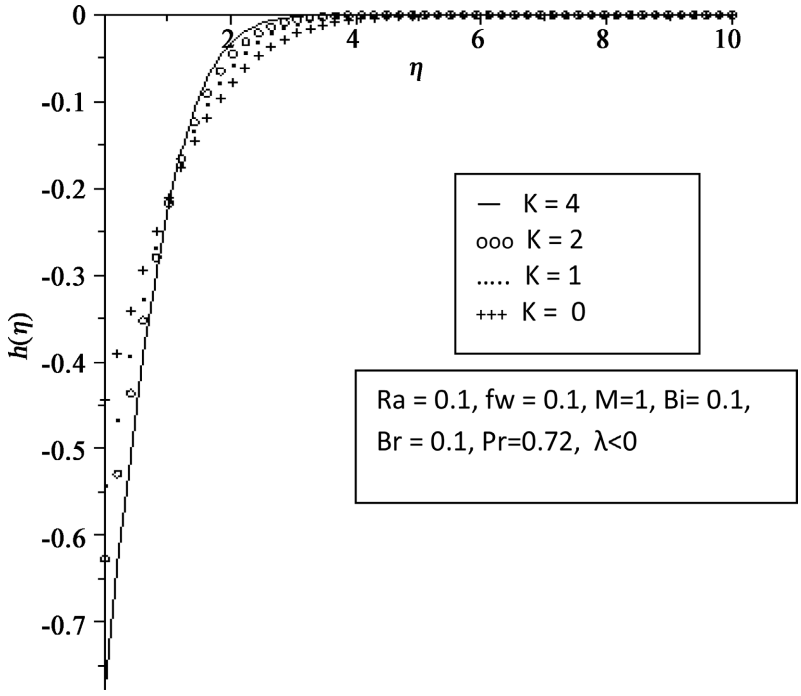

Figure 13. Microrotation profiles for vortex viscosity parameter (opposing flow).

& Figure 15, raising the magnetic parameter, causes a reduction in the thermal boundary layer thickness, and increasing suction has a similar effects. However, as seen in Figure 16, decreasing the prandtl number results in a thinner thermal boundary layer. Additionally, as demonstrated in Figures 17-19, increasing viscous dissipation, convective heat transfer, and thermal radiation, respectively,

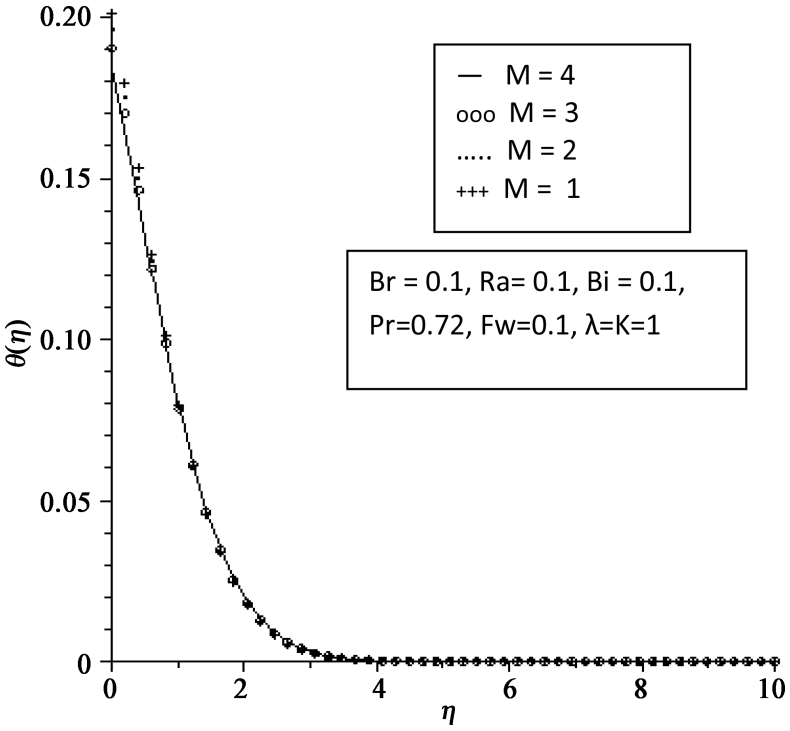

Figure 14. Temperature profiles for magnetic field parameter.

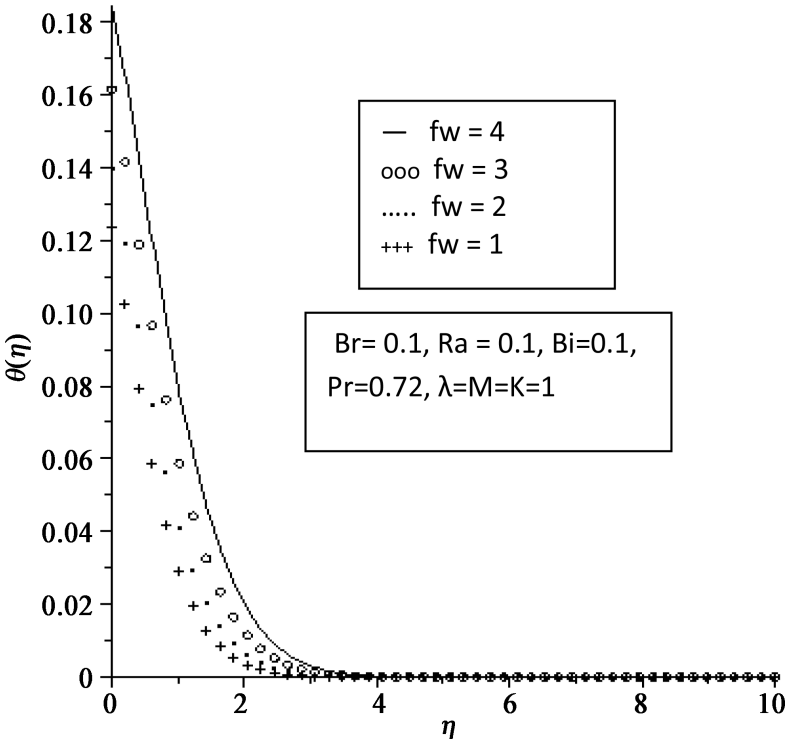

Figure 15. Profiles of temperature for the suction parameter.

raises the temperature profiles. However, increase in the vortex viscosity parameter have the effect of improving temperature profiles and thickening the thermal boundary layer in the flow field, as seen in **Figure 20** & **Figure 21**.

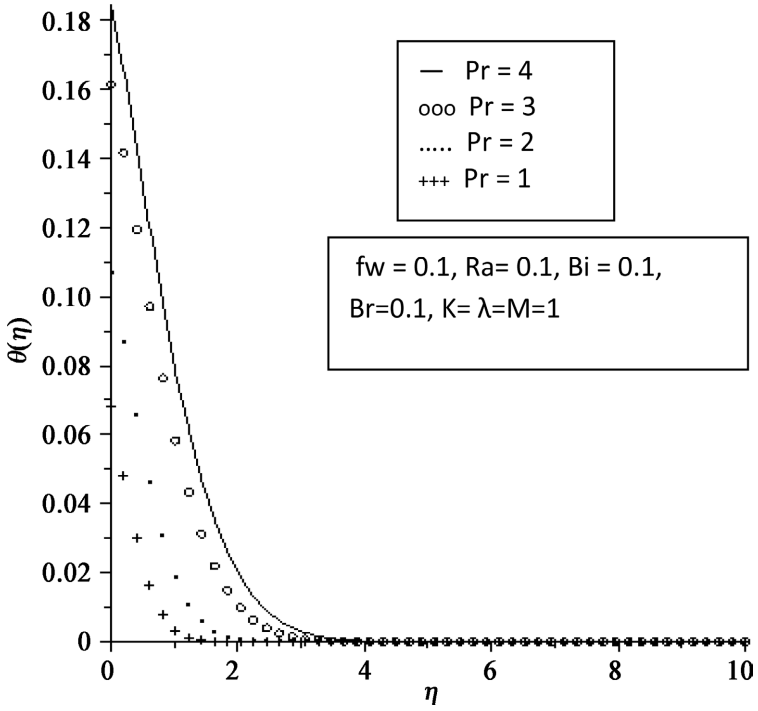

Figure 16. Profiles of temperature for the Prandtl number.

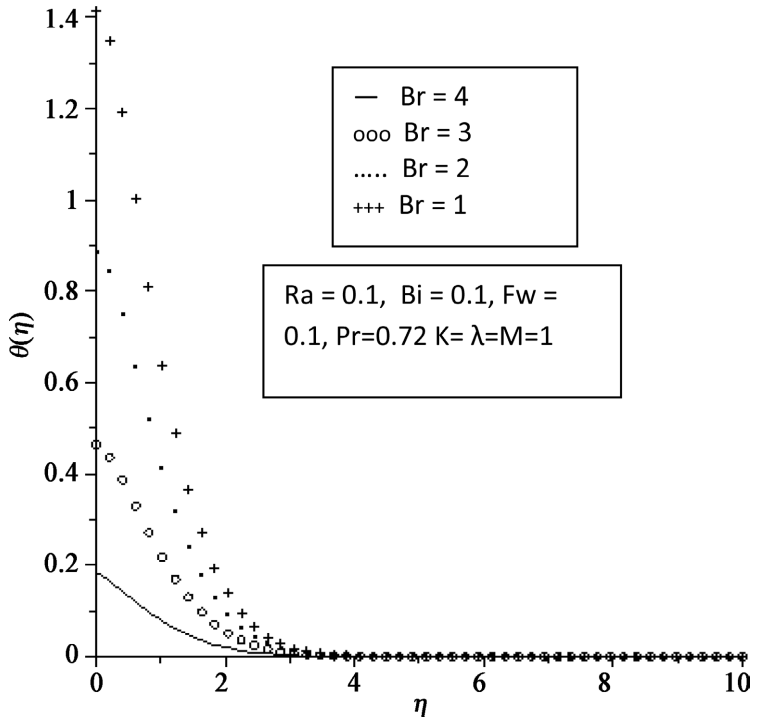

Figure 17. Profiles of temperature for the Brinkman number.

5. Conclusions

1) The vortex viscosity parameter (*K*) *causes a rise in the velocity profiles, while other parameters such as the* magnetic parameter (*M*), suction (*fw*), *Brinkmann number* (*Br*), *Biot* (*Bi*), and radiation parameter (*Ra*) cause a reduction. In

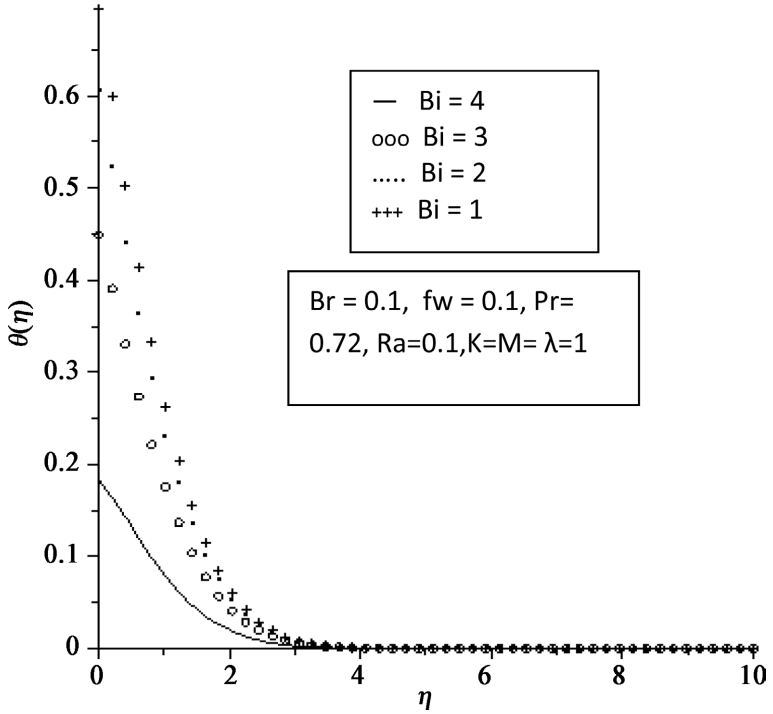

Figure 18. Profiles of temperature for the Biot number.

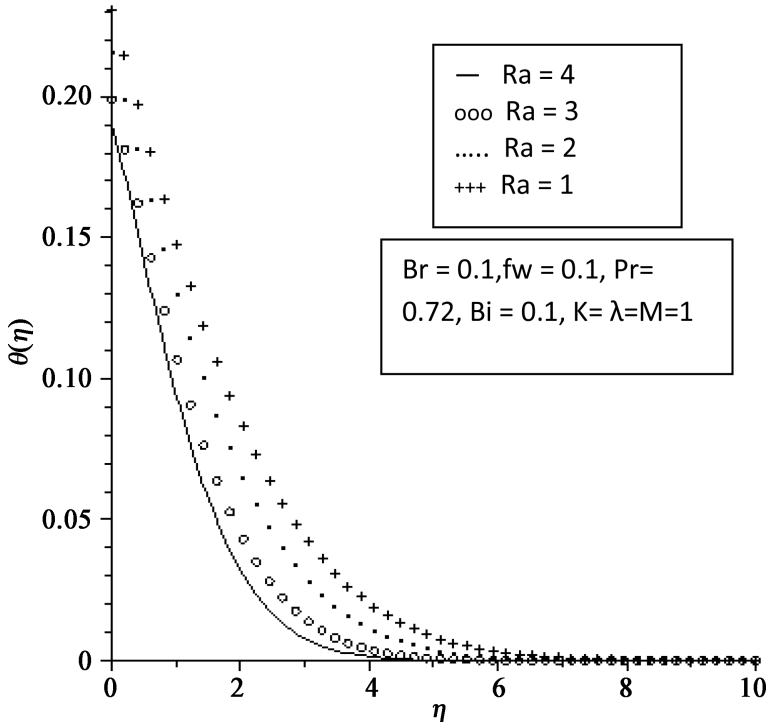

Figure 19. Profiles of temperature for the radiation parameter.

contrast, the thickness of the thermal boundary layer rises with the magnetic parameter (*M*), *Brinkmann number* (*Br*), *Biot number* (*Bi*), radiation (*Ra*) and vortex viscosity (*K*), whereas it decreases with increasing suction and prandtl.

2) The microrotation profiles decreases with increasing magnetic parameter

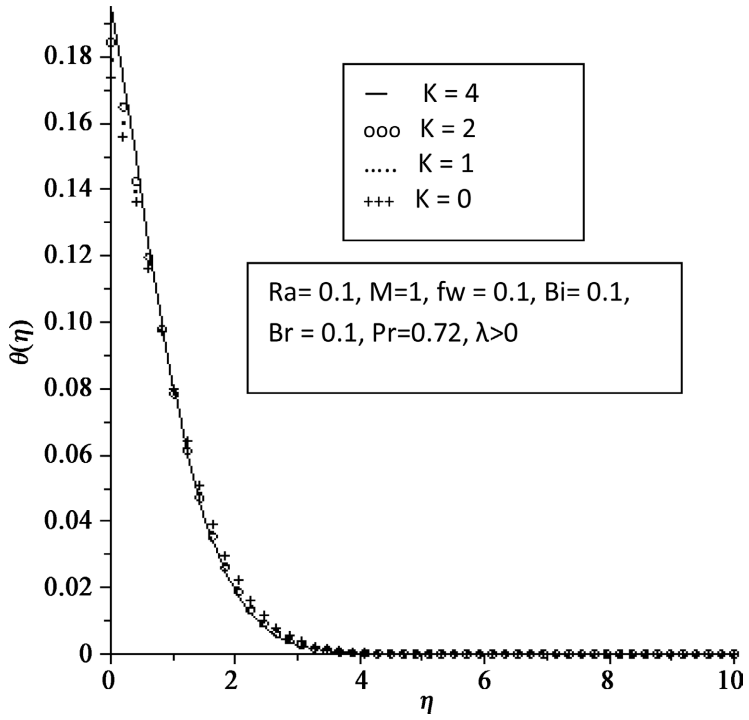

Figure 20. Profiles of temperature for the material parameter (assisting flow).

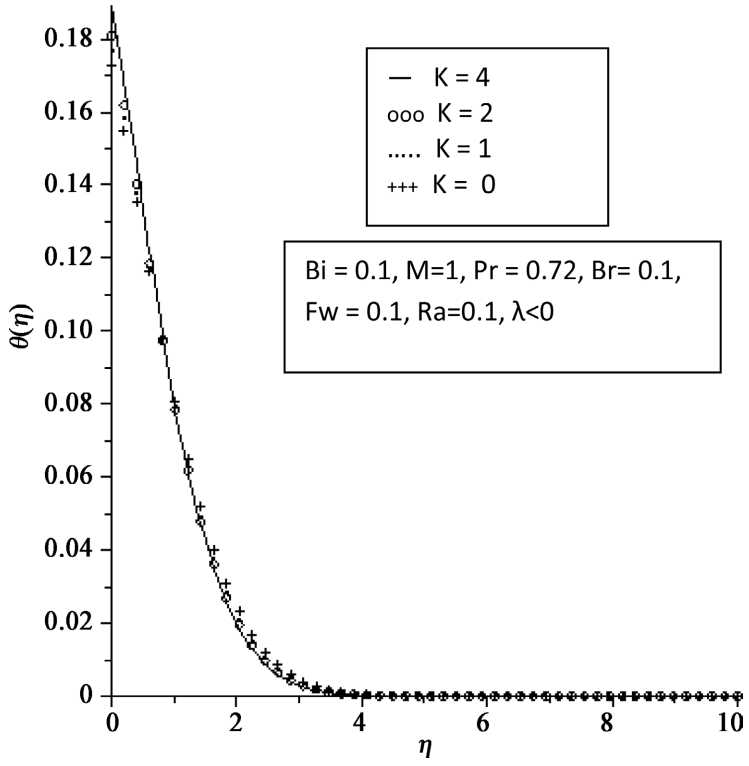

Figure 21. Profiles of temperature for the material parameter (opposing flow).

(*M*), *suction* (*fw*) and vortex viscosity (*K*) and increases with increasing Brinkmann number (*Br*) and Biot number (*Bi*).

3) Depending on whether the flow is aiding or opposing, the couple and shear

stresses at the surface are affected.

6. Suggestion for Further Study

It has been found that energy flux can be generated not only by temperature gradients but also by concentration gradients. The heat transfer caused by a concentration gradient is termed as diffusion thermo (Dufour) effect. On the other hand, mass transfer created by temperature gradients is called thermal-diffusion (Soret) effect. Generally, in heat and mass transfer process, the Soret and Dufour effects are neglected because they are smaller order of magnitude than the effects described by Fourier's and Fick's laws.

The Soret effect has been utilized for isotope separation and in mixture between gases of very light molecular weight and of medium molecular weight. Further research is recommended to include Soret and Dufour effects in the present study for a better analysis. It is also recommended that further research is done to investigate into this problem by varying the orientation of the flat plate. Particularly, an inclined plate will make this work more general.

Conflicts of Interest

The authors declare no conflicts of interest regarding the publication of this paper.

References

[1] Eringen, A.C. (1966) Theory of Micropolar Fluids. *Journal of Mathematics and Mechanics*, **16**, 1-18. https://doi.org/10.1512/iumj.1967.16.16001

[2] Ahmadi, G. (1976) Self-Similar Solution of Incompressible Micropolar Boundary Layer Flow over a Semi-Infinite Plate. *International Journal of Engineering Science*, **14**, 639-646. https://doi.org/10.1016/0020-7225(76)90006-9

[3] Soundalgekar, V.M. and Takhar, H.S. (1983) Flow of a Micropolar Fluid on a Continuous Moving Plate. *International Journal of Engineering Science*, **21**, 961. https://doi.org/10.1016/0020-7225(83)90072-1

[4] Ali, N. and Hayat, T. (2008) Peristaltic Flow of a Micropolar Fluid in an Asymmetric Channel. *Computer and Mathematics with Applications*, **55**, 589-608. https://doi.org/10.1016/j.camwa.2007.06.003

[5] Rees, D.A.S. and Pop, I. (1998) Free Convection Boundary Layer Flow of Micropolar Fluid from a Vertical Flat Plate. *IMA Journal of Applied Mathematics*, **61**, 179-197. https://doi.org/10.1093/imamat/61.2.179

[6] Sajid, M., Abbas, Z. and Hayat, T. (2009) Homotopy Analysis for Boundary Layer Flow of a Micropolar Fluid through a Porous Channel. *Applied Mathematical Modelling*, **33**, 4120-4125. https://doi.org/10.1016/j.apm.2009.02.006

[7] Hayat, T., Abbas, Z. and Javed, T. (2008) Mixed Convection Flow of a Micropolar Fluid over a Non-Linearly Stretching Sheet. *Physics Letters A*, **372**, 637-647. https://doi.org/10.1016/j.physleta.2007.08.006

[8] Hiemenz, K. (1911) Die Grenzschicht an einem in dengleichformingen Flussigkeitsstrom einge-tauchten graden Kreiszylinder. *Dinglers Polytechnisches Journal*, **326**, 321-324.

[9] Homann, F. (1936) Der Einfluss grosser Zahigkeit bei der Stromung um den Zylinder und um die Kugel. *ZAMM—Journal of Applied Mathematics and Mechanics*, **16**, 153-164. https://doi.org/10.1002/zamm.19360160304

[10] Nazar, R., Amin, N., Filip, D. and Pop, I. (2004) Stagnation Point Flow of Amicropolar Fluid towards a Stretching Sheet. *International Journal of Non-Linear Mechanics*, **39**, 1227-1235. https://doi.org/10.1016/j.ijnonlinmec.2003.08.007

[11] Zhu, J., Zheng, L.C. and Zhang, X.X. (2011) The Influence of Thermal Radiation on MHD Stagnation Point Flow past a Stretching Sheet with Heat Generation. *Acta Mechanica Sinica*, **27**, 502-509. https://doi.org/10.1007/s10409-011-0488-y

[12] Pop, S.R., Grosan, T. and Pop, I. (2004) Radiation Effects on the Flow near the Stagnation Point of a Stretching Sheet. Tech. Mech., Band 25. Heft 2, 100-106.

[13] Ibrahim, S.Y. and Makinde, O.D. (2011) Chemically Reacting Magnetohydrodynamics (MHD) Boundary Layer Flow of Heat and Mass Transfer past a Low-Heat-Sheet Moving Vertically Downwards. *Scientific Research and Essays*, **6**, 4762-4775.

[14] Christian, E.J., Seini, Y.I. and Arthur, E.M. (2014) MHD Boundary Layer Stagnation Point Flow with Radiation and Chemical Reaction towards a Heated Shrinking Porous Surface. *International Journal of Physical Sciences*, **9**, 320-328. https://doi.org/10.5897/IJPS2014.4177

[15] Ayando, T. (2015) Blasius Flow of Magnetohydrodynamic (MHD) Micropolar Fluid past a Permeable Plate with Thermal Radiation. https://www.udsspace.uds.edu.gh/jspui/handle/123456789/2280

[16] Pantokratoras, A. (2004) Effect of Viscous Dissipation in Natural Convection along a Heated Vertical Plate. *Applied Mathematical Modelling*, **29**, 553-564. https://doi.org/10.1016/j.apm.2004.10.007

[17] Lakshmi, M.P., Reddy, N.B. and Poornima, T. (2012) MHD Boundary Layer Flow of Heat and Mass Transfer over a Moving Vertical Plate in a Porous Medium with Suction and Viscous Dissipation. *International Journal of Engineering Research and Applications*, **2**, 149-159.

[18] Subhas, M.A., Sanjayanand, E. and Mahantesh, M.N. (2007) Viscoelastic MHD Flow and Heat Transfer over a Stretching Sheet with Viscous and Ohmic Dissipation. *Communications in Nonlinear Science and Numerical Simulation*, **13**, 1808-1821. https://doi.org/10.1016/j.cnsns.2007.04.007

[19] Imoro, R., Arthur, E.M. and Seini, Y.I. (2014) Heat and Mass Transfer over a Vertical Surface with Convective Boundary Conditions in the Presence of Viscous Dissipation and Nth Order Chemical Reaction. *International Journal of Computational and Applied Mathematics*, **9**, 101-118.

[20] Arthur, E.M., Seini, I.Y. and Seidu, A. (2014) On Chemically Reacting Hydromagnetic Flow over a Flat Surface in the Presence of Radiation with Viscous Dissipation and Convective Boundary Conditions. *American Journal of Applied Mathematics*, **2**, 179-185. https://doi.org/10.11648/j.ajam.20140205.15

[21] Makinde, O.D. (2011) Similarity Solution for Natural Convection from a Moving Vertical Plate with Internal Heat Generation and a Convective Boundary Condition. *Thermal Science*, **15**, 137-143. https://doi.org/10.2298/TSCI11S1137M

[22] Mamta, G., Vikas, T. and Rajendra, Y. (2017) Stagnation Point Flow of MHD Micropolar Fluid in the Presence of Melting Process and Heat Absorption/Generation. *Global Journal of Pure and Applied Mathematics*, **13**, 4889-4907.

[23] Lok, Y.Y., Amin, N., Campean, D. and Pop, I. (2005) Steady Mixed Convection Flow of a Micropolar Fluid near the Stagnation Point on a Vertical Surface. *The International Journal of Numerical Methods for Heat & Fluid Flow*, **15**, 654-670.

https://doi.org/10.1108/09615530510613861

[24] Ramachandran, N., Chem, T.S. and Armaly, B.F. (1988) Mixed Convection in a Stagnation Flows Adjacent to a Vertical Surfaces. *ASME Journal of Heat and Mass Transfer*, **110**, 373-377. https://doi.org/10.1115/1.3250494

[25] Ghasemi, S.E. and Hatami, M. (2021) Solar Radiation Effects on MHD Stagnation Point Flow and Heat Transfer of a Nanofluid over a Stretching Sheet. *Case Studies in Thermal Engineering*, **25**, Article ID: 100898. https://doi.org/10.1016/j.csite.2021.100898

[26] Lund, L.A., Omar, Z., Khan, I., Baleanu, D. and Nisar, K.S. (2020) Dual Similarity Solution of MHD Stagnation Point Flow of Casson Fluid with Effects of Thermal Radiation and Viscous Dissipation: Stability Analysis. *Scientific Report*, **10**, Article No. 15405. https://doi.org/10.1038/s41598-020-72266-2

[27] Hsiao, K.L. (2016) Stagnation Electrical MHD Nanofluid Mixed Convective with Slip Boundary on Stretching Sheet. *Applied Thermal Engineering*, **98**, 850-861. https://doi.org/10.1016/j.applthermaleng.2015.12.138

[28] Bilal, M. (2020) Micropolar Flow of EMHD Nanofluid with Nonlinear Thermal Radiation and Slip Effects. *Alexandra Engineering Journal*, **59**, 965-976. https://doi.org/10.1016/j.aej.2020.03.023

[29] Shahzada, M.A., Muhammad, A.U.R. and Homan, E. (2021) Stagnation Point Flow of Electrical Magneto-Hydrodynamic (EMHD) Micropolar Nanofluid with Mixed Convection and Slip Boundary. *Complexity*, **2021**, Article ID: 3754922. https://doi.org/10.1155/2021/3754922

[30] Ishak, A., Nazar, R. and Pop, I. (2008) Magnetohydrodynamics (MHD) Flow of a Micropolar Fluid towards a Stagnation Point on a Vertical Surface. *Computers and Mathematics with Applications*, **56**, 3188-3194. https://doi.org/10.1016/j.camwa.2008.09.013

[31] Olanrewaju, P.O., Okedayo, G.T. and Gbadeyan, J.A. (2011) Effects of Thermal Radiation on Magnetohydrodynamic (MHD) Flow of a Micropolar Fluid towards a Stagnation Point on a Vertical Plate. *International Journal of Applied Science and Technology*, **1**, 219-230.